Kuwait J. Sci. **46 (3)** pp. 90-102, 2019

Dynamic effect and stress wave analysis by transient unloading of a rock sample under high stress condition

Hongyun Yang[1,2], Shugang Cao[1,*], Guisong Zhou[2], Yong Li[1]

Ruikai Pan[1], Yuan Zhao[1], Yanbao Liu[3]

[1]*State Key Laboratory of Coal Mine Disaster Dynamics and Control, Chongqing University, Chongqing 400044, China*

[2]*China Gezhouba Group Explosive CO., LTD. Chongqing 401121, China*

[3]*China Coal Technology Engineering Group Chongqing Research Institute, Chongqing 400039, China*

** Corresponding author: shugang.cao@cqu.edu.cn*

Abstract

The strain rate equation of a rock sample end block unit was obtained during the transient unloading process, and the strain rate magnitude indicated that the rock sample had an obvious dynamic effect according to the strain rate standard of rock loading dynamics. The end unit produced a tensile stress with certain unloading times. In addition, the dynamic module of the 3DEC program and its "static stress initialization-dynamic unloading" calculation mode were used to analyze the stress propagation property after transient unloading. It was observed that the rock sample containing elastic material circularly produced high tensile and compressive stresses that were reflected at two ends of sample. The cycle period was 4 × T when the propagation time between the two ends was T. Additionally, a rock sample with elastic-plastic material displayed a plastic damage zone that was affected by tensile stress, which was produced by reflection at the fixed end. Finally, a significant finding was that the inner stress was always tensile stress and that compressive stress never appeared after the damage zone appeared. Simultaneously, the results showed that the cycle period of tensile stress was 2 × T, while the stress presented an attenuation phenomenon.

Keywords: Rock dynamics; strain rate; stress wave propagation; transient unloading.

1. Introduction

With the gradually increasing and continuous expansion to greater depths of underground rock engineering, an understanding of failure mode and failure process of the surrounding rock around man-made openings (such as tunnels, roadways and chambers) has greatly changed, and the quantifiable expression is now being investigated. High stress is superimposed and accumulated by gravity, tectonic stress or residual tectonic stress. Concentrated stress can also be caused by excavation. These changes come with aberrant ground stress in deep rock mass. A large amount of elastic strain energy can accumulate in a rock mass under high stress. Dynamic disasters can occur under these specific conditions (Hu *et al et al*., 2008; Dou *et al*., 2005).

Many researchers (Shao *et al*., 2004; Li *et al*., 2005; Li *et al*., 2007) have studied the dynamic failure characteristics and criteria based on rock loading dynamics according to stress wave theory. This has improved the theoretical awareness of rock mass dynamic disasters. Rock mass with high stress could also present dynamic phenomena in the unloading process. For instance, coal and gas bursting always occurs during the process of uncovering rock cross-cut coal in coal mines. Rock-burst can also occur during the excavation of rock roadways, tunnels, and chambers.

In the rapid unloading process of rock mass with high stress, many properties have been found to be similar to that of the rock loading dynamic. Some are even more intense, like the broken degree and damage range of a rock mass , which can be significant. Yi *et al*. (2005), Lu *et al*. (2007; 2012), Yang *et al*. (2013), Fan et al. (2015) and Yan *et al*. (2015) analyzed the mechanic effects and calculated the stress unloading duration time in the excavation process of underground rock with medium-

high stress. The researchers proposed the viewpoint of transient unloading while considering that the dynamic effect should be taken into consideration. The process of transient unloading was found to induce a vibration near the excavating surface of rock mass. It was different from that of the conventional quasi-static unloading. Further studies have shown that the vibration amplitude might exceed that of blast vibration in the surrounding rock. This phenomenon may become the main factor causing rock mass failure.

For the studying of rock unloading dynamics, numerical simulations and laboratory studies have been widely carried out. Tao *et al*. (2012; 2013) studied rock sample failure characteristics with an unloading time from 10^{-5} to 10^{-4} s using a commercial finite element program, LS-DYNA. The study was based on strain energy density (SED) rate and initial stress release rate (ISRR) theory. Huang *et al*. (2011) used RFPA2D to simulate the transient unloading confining pressure process. They found that the rock sample presented a large area of damage near the free surface and mainly presented the shear failure under a high-axial stress condition. Xu and Lu (2003) investigated the role of the dynamic unloading effect in the rock blasting process and judged the relative study to be insufficient and mostly limited to the qualitative research. He *et al*. (2007; 2014) rapidly unloaded the horizontal stress of a granite sample under three-dimensional stress condition and discovered that it presented non-linear dynamic failure phenomena. Wei *et al*. (2014) and Yang *et al*. (2014) found that the damage range of surrounding rock with high stress under the transient unloading condition was significantly greater than that of the static stress unloading process.

From the above analysis, the dynamic phenomenon of high stress rock mass caused by transient unloading has been subject to more research for the failure mechanism. The prevention and suppression of transient unloading-induced disasters and utilization of their failure mechanism for rock breaking is thus an important research topic. This is especially true for deep well gas drilling. However, most research results were obtained via qualitative analysis of the apparent phenomena, which is not a significantly accurate way to analyze the essential cause of this dynamic effect. Additionally, the unloading process is difficult to control for unloading failure of rock in a laboratory. This leads to special data in the unloading process of deep underground rock which cannot be ascertain to interpret the dynamics of the phenomenon.

In this paper, a theoretical analysis based on dynamics theory was utilized to evaluate the characterization parameters of unloading dynamics, including rock strain rate (RSR) and acceleration. Then a dynamic module of the 3-dimensional distinct element code (3DEC) was employed to simulate inner stress, and its propagation property in rock sample with elastic-plastic material, and finally discuss the failure mechanism of rock mass.

2. Dynamic parameters analysis of transient unloading

It is generally believed that a rock sample will produce some vibrations when the RSR is more than 1×10^{-3} s^{-1}. An RSR between 1×10^{-1} and 1×10^{4} s^{-1} belongs to the rock load dynamics field, and the rock dynamic action time is at a microsecond (μs) and millisecond (ms) level (Field *et al*., 2004; Huang, 2011). In addition, in the rock dynamic field, the typical load is the impulse load and the inertial effect must be considered. This means that high acceleration will be produced (Bin *et al*., 2013). Therefore, RSR and acceleration are two important parameters to characterize dynamics, and their value size will be described in detail.

2.1 Model for transient unloading

To solve for the unloading dynamic parameters, the displacement solution must be obtained. But, first, the unloading model and unloading path must be determined.

2.1.1 Rock sample unloading model

In reality, an underground rock mass is in a 3D stress state, but the unloading process of the rock mass under 3D initial stress is very complex. Thus, the analytical solution of displacement might be impossible for any statically indeterminate system. Therefore, it is complicated to use 3D-modelling to solve this problem. However, man-made opening excavations only operate in one direction (Tao *et al*., 2012). To simplify the problem, the model is stress-free, i.e., the confining stress is zero, which simplifies this case to a 1D-stress state problem when characterizing the transient unloading process under axial initial stress only (Tao *et al*., 2012). Therefore, the unloading process is estimated by using a rock sample with isotropic material (Figure 1).

It is assumed that the rock sample in Figure 1 has being compressed based on the stress state of underground rock mass, and has initial compression deformations The magnitude of the initial deformations mainly depends on the magnitude of the deformations produced by the initial stress. Assume the stress is applied along the x-direction and there is an initial equilibrium, the relationship of stress and deformation can be expressed by Equation

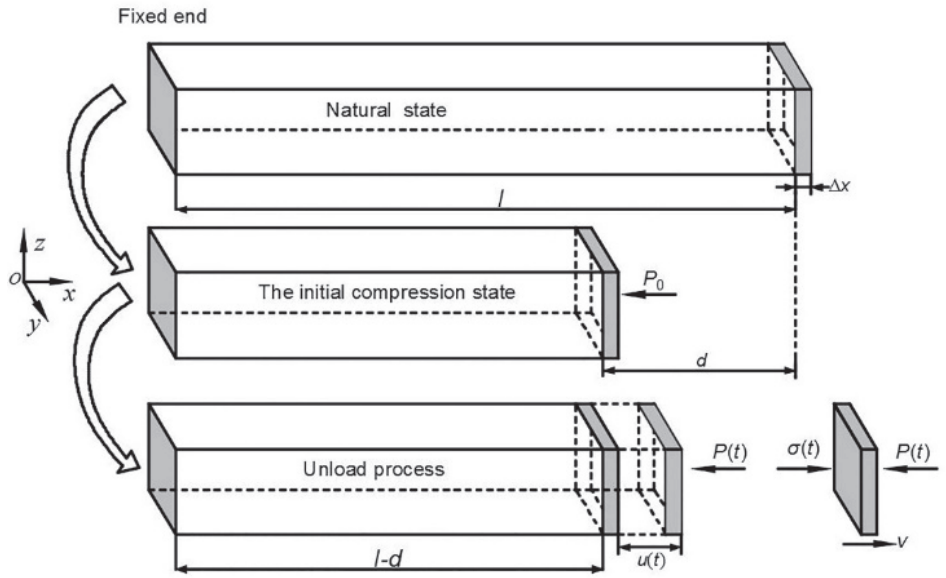

Fig. 1. Rock sample unloading model

(1a). Then it is also unloaded in the same direction. For the model (Figure 1), l is the initial length of the sample before compressing. Δx is the end unit length, d is the maximum compression deformation under the action of P_0, and *u(t)* is the displacement of the end unit for sample compression state. Furthermore, $\sigma(t)$ is the left end stress of this unit in unloading process, which was produced by deformation and expressed by Equation (1b). The dynamics relationship for the end unit in the unloading process is shown in Equation (1c).

$$\begin{cases} E\dfrac{d}{l} = P_0 & (a) \\ \sigma(t) = E\dfrac{d-u(t)}{l} & (b), \\ \sigma(t)\cdot s - P(t)\cdot s - m\cdot\ddot{u}(t) = 0 & (c) \end{cases} \quad (1)$$

where E is the elastic modulus of the material, ρ is the sample density, and s is the area size of sample cross

section..

2.1.2 Path for transient unloading

The different excavation methods can be characterized by different initial stress unloading paths. The paths of stress transient unloading for a rock mass can be fitted by a linear, negative exponential and a 1/4 cosine function, as shown in Fig. 2 (Lu *et al*., 2008). The functions can be observed in Equations (2), (3) and (4), respectively.

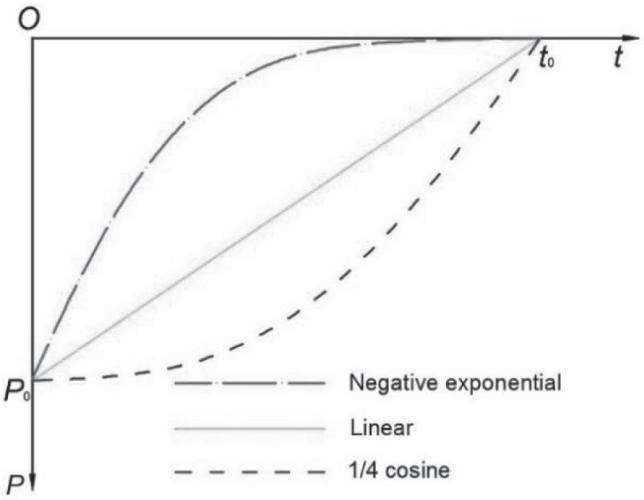

Fig. 2. Paths for transient unloading of in-situ stress

$$P(t) = P_0\left(1\text{-}t/t_0\right) \quad (2)$$

$$P(t) = P_0 e^{(-\beta t/t_0)} \quad (3)$$

$$P(t) = P_0\cos(\pi t/(2t_0)), \quad (4)$$

where *P(t)* is the external pressure stress in the unloading process, P_0 is the in-situ stress, t_0 is the duration time of unloading, and β is the attenuation exponent. To simplify the calculation procedure, the linear unloading path is used for the calculations.

2.2 Displacement solution

According to Equations (1) and (2), the following physical equation is obtained:

$$\rho \cdot \Delta x \cdot \ddot{u}(t) + \frac{E}{l} u(t) - P_0 \cdot \frac{t}{t_0} = 0 \tag{5}$$

Equation (5) is a 2-order, non-homogeneous, linear ordinary differential equation, the boundary conditions of which are as follows:

$$\begin{cases} u|_{t=0} = 0 \\ \dot{u}|_{t=0} = 0 \end{cases} \tag{6}$$

After using the method of variation of the constant, the displacement analytical solution for Equation (5) is obtained, as follows:

$$u(t) = \frac{-l\sqrt{l} \cdot P_0 \sqrt{\rho \cdot \Delta x}}{E\sqrt{E} \cdot t_0} \sin\left(\sqrt{E/(\rho l \cdot \Delta x)} \cdot t\right) + \frac{lP_0}{Et_0} \cdot t \tag{7}$$

$$(0 \le t \le t_0)$$

It can be found that the density ρ and the elastic modulus E for a specific material are constant. The end block unit length Δx and rock sample length l were subjectively selected, which has a great impact on the displacement.

To produce results with a certain precision and comparability, the length Δx = 0.001 m, l = 1 m, and the physical and mechanical parameters of sandstone and the model parameters were used, as listed in Table 1. In addition, it was determined that the MPa and the value of $t_0 = 3 \times 10^{-5}$ s, 5×10^{-5} s, 7.5×10^{-5} s, 1×10^{-4} s, 2.5×10^{-4} s and 5×10^{-4} s. This allowed for the displacement changing curves under 6 different unloading times to be calculated (Figure 4).

Table 1. Physical and mechanical parameters of sandstone and calculated model parameters

Lithology	Density P (kg/m^3)	Uniaxial compression strength σ_c (MPa)	Uniaxial tensile strength σ_t (MPa)	Cohesion c (MPa)	Internal friction angle φ (°)	Poisson's ratio	Elasticity modulus E (GPa)	Dilation angle ψ (°)
Sandstone	2630	62.77	7.48	10.83	51.91	0.153	24.3	10
Model	l(m)	Δx(m)	P_0(MPa)	$t_0 \times 10^{-4}$ (s)				

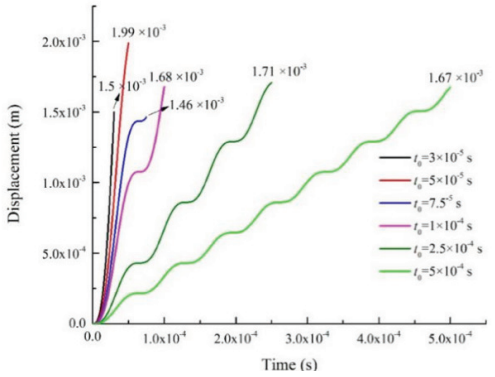

Fig. 3. Displacement functional image

Figure 3 shows: (1) the time difference is more than ten-fold from $t_0 = 3 \times 10^{-5}$ s to $t_0 = 5 \times 10^{-4}$ s, but the displacement does not change by much. This illustrates that the displacement, when the unloading time ends, is not sensitive to the unloading time of t_0.; (2) the shorter the unloading time of t_0, the greater the displacement increases the rate; and, (3) the presence of more obvious displacement volatility curves and strong nonlinear properties illustrates that a certain degree of vibration was produced during the unloading process, which is consistent with the micro-quake events produced in the field transient unloading process. See detailed researched by Lu *et al*. (2007); Lu *et al*. (2012); Yang *et al*. (2013).

2.3 Strain rate analysis

To study the RSR evolution law in the transient unloading process to determine whether it reaches the strain rate magnitude of the rock loading dynamic, the RSR is calculated as follows:

$$\dot{\varepsilon}(t) = \frac{d\varepsilon(t)}{dt} = \frac{d\left(u(t)/(l-d)\right)}{dt} = \frac{du(t)}{(l-d) \cdot dt} = \frac{v(t)}{(l-d)} \tag{8}$$

In Equation (8), $v(t)$ is the speed of the end block unit. Through further analysis, according to Equations (7) and (8), the strain rate expression is derived as follows:

$$\dot{\varepsilon}(t) = \frac{-P_0}{(E-P_0)t_0} \cos\left(\sqrt{E/(\rho l \cdot \Delta x)} \cdot t\right) + \frac{P_0}{(E-P_0)t_0} \tag{9}$$

assuming that:

$$t_n = \pi \cdot \sqrt{\rho l \cdot \Delta x} / \sqrt{E}\,. \tag{10}$$

By using the data in Table 1, it is found that $t_n = 3.27 \times 10^{-5}$ s. It can be observed that when t_0 satisfies $0 \le t_0 \le t_n$, the maximum strain rate can be calculated by using Equation (9). When t_0 satisfies $t_0 \ge t_n$, the maximum strain rate can be calculated by using Equation (11):

$$\varepsilon_{max} = \frac{2P_0}{(E-P_0)t_0} \quad (t_0 \ge t_n) \tag{11}$$

By using Equations (9) and (11), the relationship of RSR and its maximum value with 6 different unloading times was computed, as shown in Figure 4.

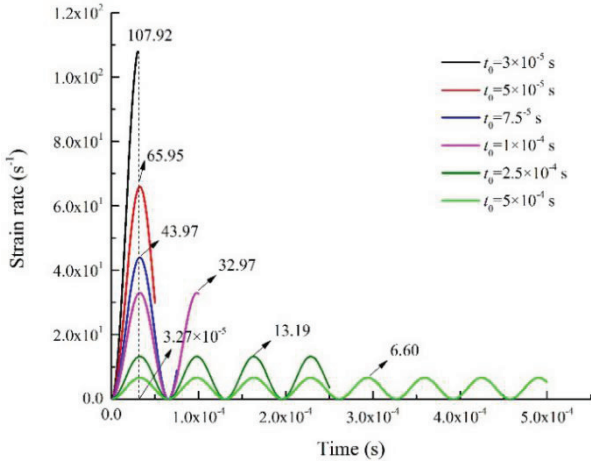

Fig. 4. Image of the RSR function

Figure 4 shows that the strain rate curve fluctuates more obviously, and the maximum strain rate decreases as total unloading time t_0 increases. On the contrary, the smaller the value of t_0, the larger the maximum strain rate. Further analysis indicates that the minimum strain rate is 6.6×10^0 s^{-1} and the maximum strain rate is 1.0792×10^2 s^{-1}, whose values reach the strain rate magnitude of rock loading dynamics.

Previous studies have shown that deep underground rock bears overburden stress, concentration stress and tectonic stress, which tend to be greater. According to the stress measurement from a study completed in South Africa, the stress at a burial depth from 3500 to 5000 m can reach 95 to 135 MPa (He *et al*., 2005). On the other hand, the unloading time will be shortened using particular excavation methods. We can find that the strain rate parameter values were more conservative in the above calculation process, and if the stress increased and unloading time decreased, the RSR would become greater in the transient unloading process, while the unloading dynamic effect would be more intense.

2.4 Acceleration analysis

According to the D'Alembert principle, it is the inertia force that retains an object's original motion state tendency of the particle system dynamic process, and whose value can be measured using the acceleration. Through the analysis the following relationship was found between the acceleration and RSR:

$$\ddot{u}(t) = \ddot{\varepsilon}(t) \cdot l\left(1 - P_0 / E\right) \tag{12}$$

It can be observed that the RSR and the acceleration are not two independent variables. Their relationship can be established using the rock length l, the pressure stress P0 and the elastic modulus E.

Utilizing Equation (12), the relationship of acceleration with 6 different of unloading times was computed, as shown in Figure 5.

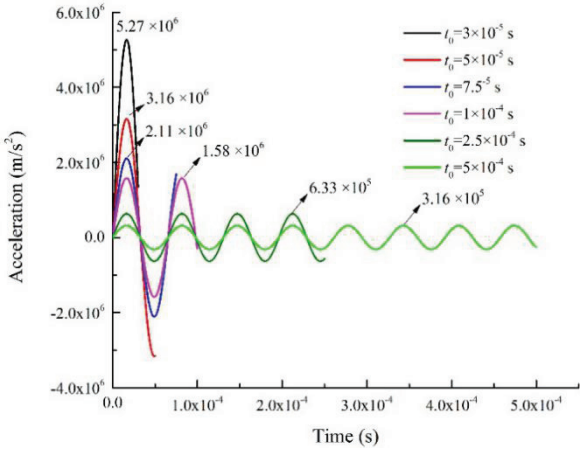

Fig. 5. Image of acceleration function

Figure 5 shows that the smaller the total unloading time t_0, the bigger the maximum acceleration. When t_0 satisfies $t_0 \geq t_n/2$, the maximum acceleration can be calculated as follows:

$$\ddot{u}(t) = \frac{P_0}{t_0} \cdot \sqrt{\frac{l}{E\rho\Delta x}} \tag{13}$$

The data in Figure 5 show that the acceleration can reach 10^5 m/s^2 when the RSR satisfies the rock dynamics category in the transient unloading process.

3. Stress evolution law

The intensity of the dynamic effect in the transient unloading process was measured by using the RSR. Generally, the maximum deformation and the RSR will appear at the end block unit. Thus, there is a strong representative significance for studying the RSR of the end block unit, as has been done in this research. Moreover, it is known that a rock sample that produces the dynamic effect will also produce dynamic deformation and damage. In reality, it will stimulate a stress wave in the unloading direction in the transient unloading process that will also propagate along the unloading direction (Tao *et al*., 2012; Tao *et al*., 2013; Carter and Booker, 1990). This can be reflected through a numerical simulation. Therefore, the following will be the study of the stress propagation property in an elastic material and an elastic-plastic material.

3.1 Stress evolution features in an end block unit

To study the stress propagation property, it is first necessary

to understand the stress evolution property of an end unit. We took the 6 different unloading times shown in Table 1 and the end pressure stress P_0 = -50 MPa. Using these, we obtained the stress $\sigma(t)$ evolution characteristic according to Equations (4) and (7) (Figure 6.)

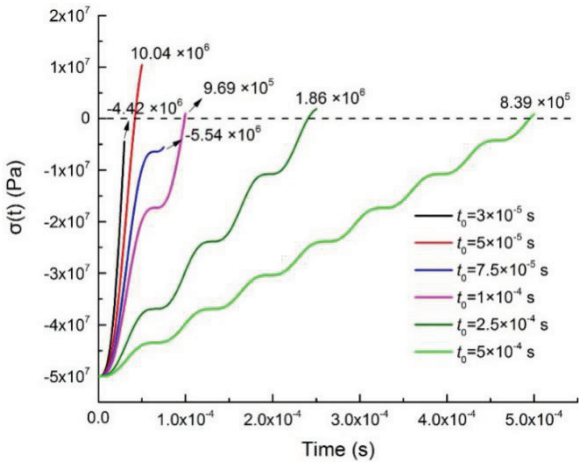

Fig. 6. The end unit stress evolution rule

Figure 6 shows: (1) the stress $\sigma(t)$ gradually decreases as the unloading time increases, and the shorter the unloading time, the greater the decrement in stress; (2) the tensile stress is produced in the final stages under some unloading times condition; and, (3) the maximum tensile stress value was 10.04 MPa, which is much higher than any tensile strength of rock.

3.2 Stress wave propagation

3.2.1 Numerical model

The study for the theoretical calculation of stress was conducted for the end unit, which can only represent the end unit stress behavior characteristics (SBC). It cannot describe the SBC in the remaining part of the model. This paper used the dynamic module of the 3DEC (Cundall, 1988; Hart *et al*., 1988) to find the SBC in the transient unloading process. To simplify the modeling procedure, a square (Tao *et al*., 2013) 3DEC rock sample model with no confining stress (Tao *et al*., 2012) is shown in Fig. 7. The physical and mechanical parameters are listed in Table 1. Calculation was performed by using the "static stress initialization-dynamic unloading" calculation mode. This means that the dynamic module is first turned off and the initial balance in the static state is calculated. After that, the dynamic module is turned on, and P_0 is linearly unloaded at the free end. The damping effect was not considered in the calculation process. At the same time, eleven stress monitoring points (A-K) were arranged in the center of model cross section in order to obtain the stress σ_x .

In general, the velocity of the wave of the rock sample in Table 1 is found as follows:

$$c = \sqrt{\frac{E}{\rho}} = 3040 \text{ m/s} \ , \tag{14}$$

where E is the elastic modulus of the rock and ρ is the density. The actual propagation time T of the wave from right to left is calculated as follows:

$$T = \frac{l}{c} \approx 3.3 \times 10^{-4} \text{ s} \tag{15}$$

3.2.2 Stress wave propagation in elastic material

The material was set with elastic constitutive relationships. The initial boundary axial pressure is P_0 =-50 MP, and the unloading time t_0 is 5×10^{-5} s. To fully show the stress wave propagation characteristic for subsequent analysis, a simulation time of $8\times T$ was taken. Furthermore, we acquired the stress nephogram of σ_x at the moment of unloading completion and $T/2$. The acquired interval $T/2$ time slot after calculating $T/2$, within the time of $4\times T$, was also calculated (Figure 8).

The following can be observed from Figure 8:

1. The compressive stress value of the rock sample decreases from the stress S_{p1}. Tensile stress occurs at the moment that unloading is finished, i.e., t = 3.3 × 10^{-4} s, and begins to spread to the fixed end from the free end, which presents a gradually increasing trend. The tensile stress at the fixed end becomes S_{t2} and that at the free end is maintained at S_{t1}.
2. High tensile stress S_{t3} is instantly produced when the stress wave is reflected at the fixed end, and the

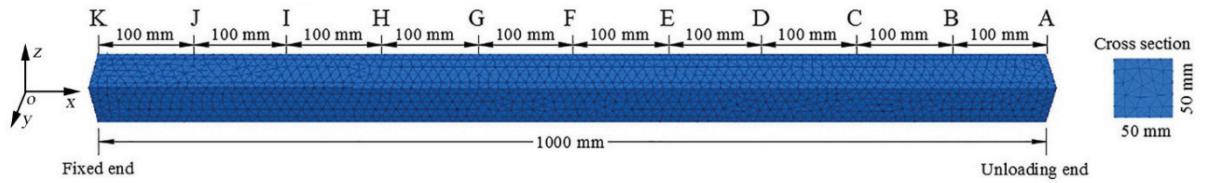

Fig. 7. Figure of numerical sample

stress value reaches 50 to 60 MPa. This value range is several times higher than the incident stress wave S_{t2} and far more than the tensile strength of rock.

3. Reflected stress wave S_{t3} propagates to the free end at $t = 6.6 \times 10^{-4}$ s. After being reflected at the free end, the tensile stress forms a low strength compressive stress S_{p2} and propagates to the fixed end, continuously increasing in the propagation process.

4. The compressive stress S_{p2} spreads to the fixed end at $t = 9.9 \times 10^{-4}$ s, and high compressive stress S_{p3} appears after Sp2 is reflected at the fixed end. It is far greater than S_{p2} and propagates to the free end. At $t = 13.2 \times 10^{-4}$ s, S_{p3} spreads to the free end and begins to spread to the fixed end after reflection. The next cycle begins, and we can observe that the cycle period is $4 \times T$.

Based on the above analysis, it is obvious that the tensile and compressive stress are produced after reflection and are sometimes higher, presenting a cycle period. (See the cyclic graph in Figure 9.)

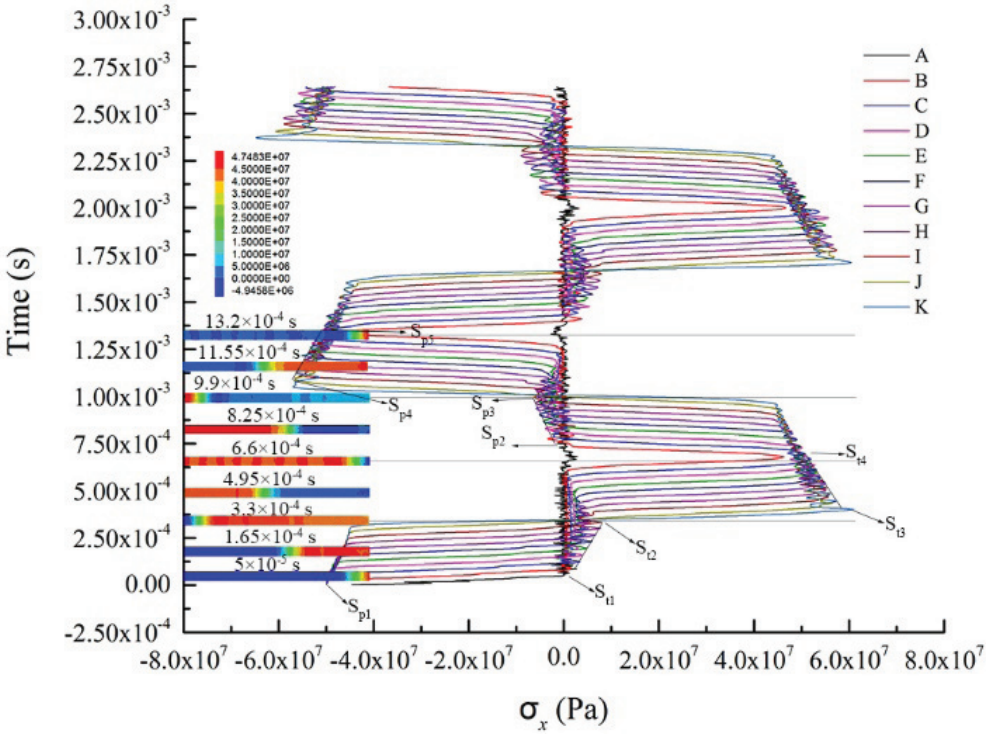

Fig. 8. Elastic materials stress propagation properties

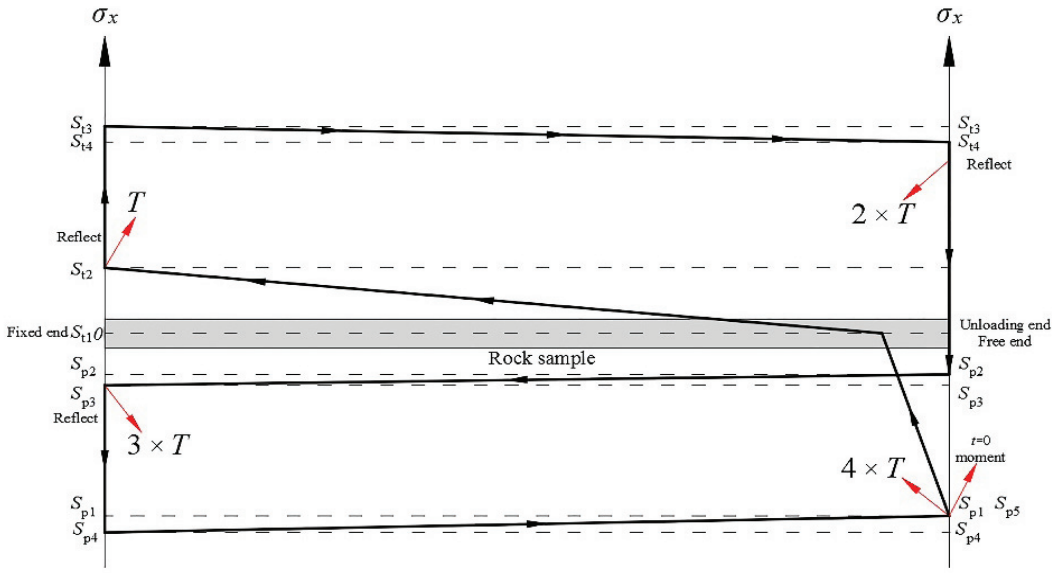

Fig. 9. Cyclic graph of σx in elastic materials

2.3 Stress propagation in elastic-plastic material

To study the failure and stress propagation characteristics of the rock sample caused by transient unloading, the Mohr-Coulomb failure criterion was used on the basis of the above rock sample and its size (Figure 7). The boundary conditions, unloading method and unloading time are the same as those in Section 3.2.2. The rock sample plastic zone was monitored in the calculation process. The results are shown in Figure 10.The following can be determined from the results:

1. Tensile stress is produced between the moment of unloading and t = 3.3 × 10^{-4} s. It continuously increases during the spread process, being S_{t2} when reaching the fixed end. However, due to the smaller tensile stress, the first three rock samples did not appear in the plastic zone.

2. The tensile stress is reflected at the fixed end and results in high tensile stress. The high tensile stress value is greater than the rock sample tensile strength, causing the damage. Meanwhile, the failure zone prevents tensile stress from continually increasing. Instead it remains at the S_{t3} level.

3. The high tensile stress continue to spread along the unloading end direction and results in a larger area of damage. However, as time progresses, much of the elastic energy is consumed, and the plastic zone is essentially unchanged.

4. The attenuated tensile stress propagates to the free end and continuously decreases, being St4 when reaching the free end. S_{t4} is reflected at the free end and is reduced. However, it gradually increases during the process of spreading to the fixed end. The next cycle begins with a cycle period of 2 × *T*. The stress cycle graph can be simplified as shown in Figure 11.

Further analysis reveals that σx is always tensile stress. In other words, it never appears as compressive stress. The tensile stress near the fixed end continuously attenuates during the cycle process due to the energy consumption in plastic zone, showing an attenuation angle α. (See Fig. 10.)

4. Discussion

4.1 RSR

For an actual underground rock mass engineering, the rock block near the free face has the maximum RSR in the transient unloading process. Therefore, the research on the dynamic parameter that is focused on a rock sample end block unit has rationality. However, it must be taken into account that the underground rock mass is in the 3-dimensional stress state, the constitutive equation of which in the x direction is:

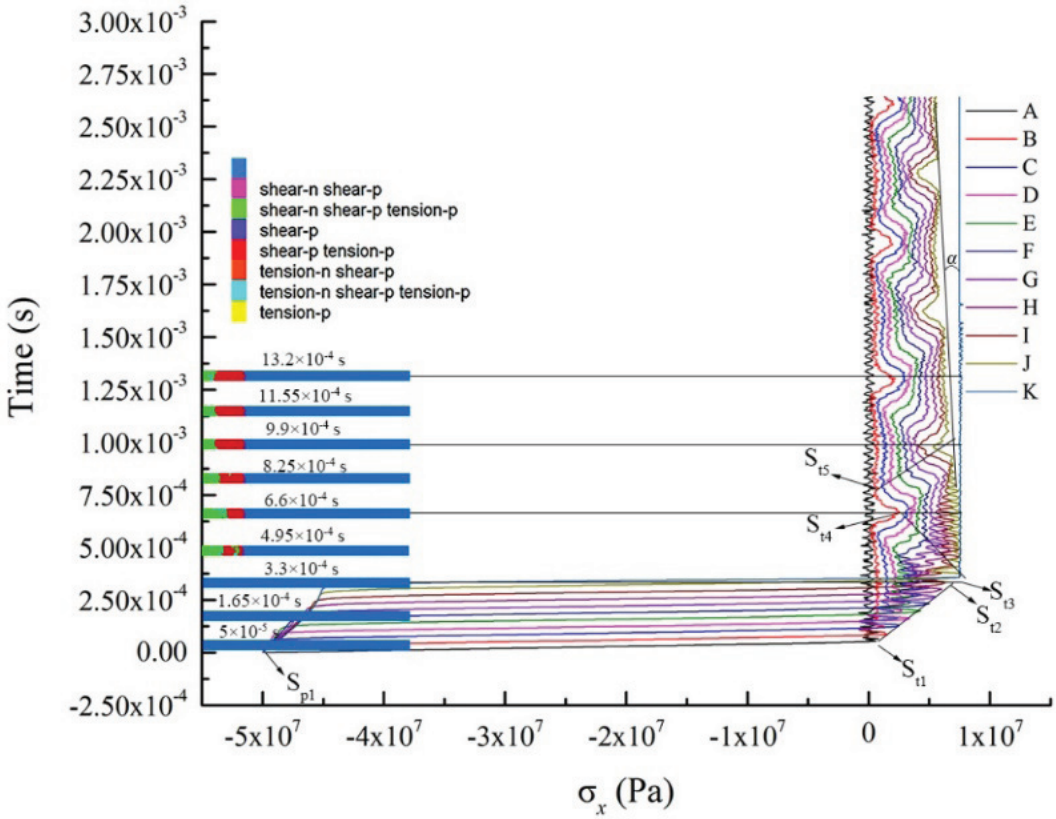

Fig. 10. Elastic-plastic materials damage and stress propagation properties

$$\varepsilon_x = \frac{1}{E}\left[\sigma_x - \mu\left(\sigma_y + \sigma_z\right)\right] \quad (16)$$

Here, the sign of σ_x is positive, while σ_y and σ_z are negative for transient unloading. The strain ε_x will become larger in the 3-dimensional stress state, as well as the RSR. Therefore, the RSR calculated using Equation (9) is conservative, meaning that the real RSR should be multiplied by a coefficient λ, where $\lambda \geq 1$.

Furthermore, from Equation (9), we can observe that the RSR can be expressed as follows:

$$\dot{\varepsilon}(t) = f(P_0, E, \rho, l, \Delta x, t_0) \quad (17)$$

Equation (17) clearly indicates that the RSR is relevant to many factors. Among the factors, the parameters P_0, E, ρ and t_0 are constant in certain geological environments and excavation conditions. However, the selection of l and Δx involves subjectivity, which has a great impact on the result of RSR. Here, an analysis is necessary.

1. It is known that the rock mass is not a continuous media. It is distributed in complex joints and fractures that cut the rock blocks into different sizes, resulting in block size differences and uncertainty. The size selection of l is intended to explain the unloading dynamic effect and should be easy to calculate. Therefore, l of 1000 mm is reasonable. Moreover, the function of these interfaces acts as the fixed end of the rock sample in the actual process, and the stress wave is reflected at the interface surface in the unloading process.

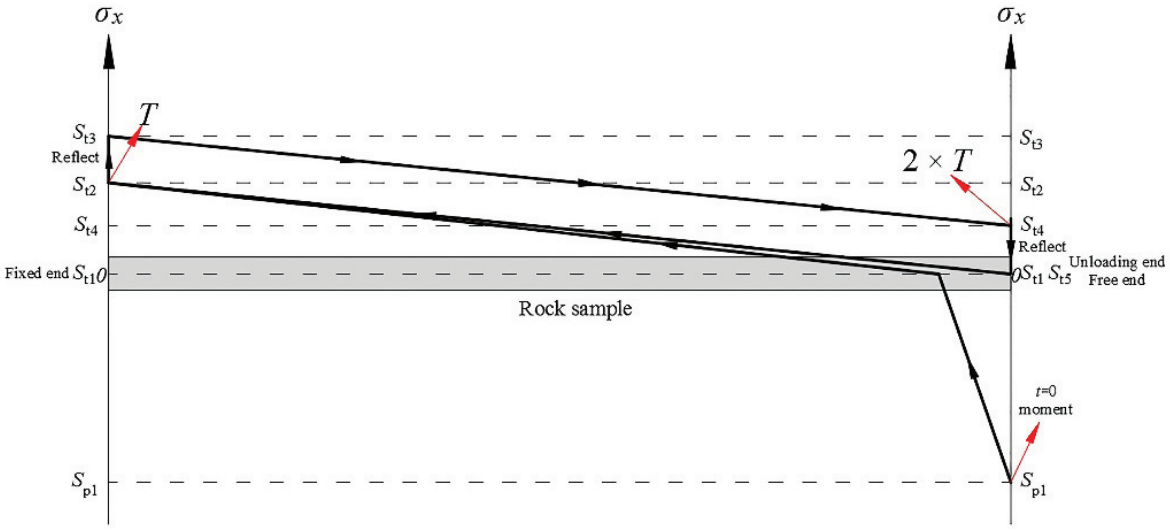

Fig. 11. Cyclic graph of σx in elastic-plastic materials

2. As a matter of fact, P_0 is equal to the in-situ stress σ along the excavation direction, and the maximum RSR expression can be changed to the following:

$$\dot{\varepsilon} = \lambda \frac{2\sigma}{(E-\sigma)t_0} \quad (\lambda \geq 1) \quad (18)$$

Equation (18) shown that the influence of l and Δx can be eliminated. The use of this equation to calculate the RSR in the transient unloading process might be inaccurate. In reality, it is difficult to draw an accurate solution for a real engineering situation. Therefore, it is viable to estimate the RSR and evaluate the dynamic effect for transient unloading under a certain geological condition by using this equation, generally considering the coefficient as λ = 1. Of course, a three-dimensional model can be developed for such research.

4.2 Failure mechanism

For the "unloading failure" phenomenon, several researchers (Poncelet, 1946; Johnson *et al.*, 1973; Atkinson, 1984; Kimberley *et al.*, 2010) have documented the initiation and propagation of cracks using brittle material specimens, such as glass and single crystal quartz. The cracks originated at the specimen boundaries and propagated into the bulk of the specimen during the unloading phase despite the lack of global tensile stresses applied to the specimen. The cracks provided a mechanism for failure and damage growth in brittle solids that had been loaded below their compressive strengths. Michelle and Erland (1994) found that cracks did not form when ice was unloaded slowly. Rather, the unloading cracks were transverse to those formed while loading and appeared as transgranular spurs to the loading cracks during rapid unloading. These were attributed to the development of tensile stresses during the unloading.

Tonge *et al*. (2012) conducted finite element simulations of uniaxial compression experiments on single crystal quartz. The research indicated that a slip-stick mechanism, which is highly dependent on interface friction, can be responsible for the generation of tensile stress states, thus leading to failure during unloading.

The simulation results in this research study show that the tensile stress is generated at the fixed end and free end. The value of the tensile stress may be beyond the tensile strength of intact rock. It either results in rock failure or generates new cracks. On the other hand, the sample end face can be treated as the crack interface. Thus, the crack interface could produce tensile stress, which may be sufficient to initiate crack growth. In addition, our simulations examined the experiments of unloading failures (Kimberley *et al*., 2010) in an anisotropic specimen of single crystal quartz. Significant tensile stresses developed which made crack growth more likely to occur (Tonge *et al*., 2012).

This research posists a brief analysis of the failure mechanism of rock during the dynamic unload phase. In fact, the failure mechanism and failure criterion of unloading are quite complex, the reason being that a united knowledgebase has not yet been formed. Figure 6 showed that the tensile stress had a significant relationship with the unloading time, which can be understood by using Equations (4) and (7). Therefore, further investments in studying these phenomena should have a positive effect on disasters prevention from rock breaking.

4.3 Model parameters

It should also be mentioned that the physical and mechanical parameters of rock in the unloading process were kept constant. However, as the parameters changed, the elastic modulus E increased (Li *et al*., 2015) in the process of rock loading dynamics. Another issue is that for transient unloading, the way in which parameters, such as elastic modulus E, Poisson's ratio μ, etc., change has rarely been studied. Ergo, an completely accurate answer cannot be calculated. Therefore, this aspect requires further research in order to make a contribution to rock unloading dynamics.

5. Conclusions

The research investigated the theoretical calculation of dynamics parameters and stress propagation property analysis for a rock sample during transient unloading. This paper had the following primary conclusions. First, the RSR equation was formulated based on the displacement analytic solution of a rock sample end unit with high stress. Second, the theoretical calculation results showed that the RSR can reach the strain rate category of rock load dynamics. This indicated that a high-stress rock can present dynamic effects in transient unloading process. In addition, the RSR was not independent to acceleration, which can reach 10^5 m/s2 magnitude. Third, the end unit produced a tensile stress with certain unloading times. Fourth, the sample with elastic material produced tensile stress and propagated inside the rock sample after transient unloading. After that, the inner stress was constantly reflected at the sample two ends where high tensile and compressive stress periodically formed. At this point, the cycle period was $4\times T$ when the propagation time between the two sample ends was T. On the other hand, the rock sample with elastic-plastic material produced a plastic damage zone at the fixed end, causing high tensile stress to form though reflecting. This plastic damage zone remained almost in the same range due to decreased tensile stress. The inner stress was basic tensile stress and the compressive stress never appear. Finally, the inner stress had a cycle period of $2\times T$ and presented an attenuate phenomenon in each cycle.

ACKNOWLEDGMENTS

The authors gratefully acknowledge funding by the National Natural Science Foundation Project of China (51474039, 51404046, U1361205), Chongqing Postdoctoral Research Project (Xm2017117), Chongqing Technological Innovation and Application Demonstration Project (cstc2018jscx-msybX0067).

Reference

Atkinson, B., Kean. (1984). Subcritical crack growth in geological materials. Journal of Geophysical Research, **89**: 4077-4114.

Bin, L., Fei, X., and Li Z. (2013). Effect and farcture analysis of inertia on dynamic void growth process of ductile metals. Journal of Mechanical Strength, **35**: 219-225.

Carter, J.P. and Booker, J.R. (1990). Sudden excavation of a long circular tunnel in elastic ground. International Journal of Rock Mechanics and Mining Sciences & Geomechanics Abstracts, **27**(2): 129-132.

Cundall, P.A. (1988). Formulation of a three-dimensional distinct element model—Part I. A scheme to detect and represent contacts in a system composed of many polyhedral blocks. International Journal of Rock Mechanics and Mining Sciences & Geomechanics Abstracts, **25**(3): 107-116.

Dou, L.M., Lu, C.P., Mou, Z.L., Qin, Y.H., and Yao, J.M. (2005). Intensity weakening theory for rockburst and its application. Journal of the China Coal Society, **30**(6): 690-694.

Fan, Y., Lu, W.B., Yan, P., Chen, M., and Zhang, Y.Z. (2015). Transient characters of energy changes induced by blasting excavation of deep-buried tunnels. Tunnelling and Underground Space Technology, **49**(0): 9-17.

Field, J.E., Walley, S.M., Proud, W.G., Goldrein, H.T., and Siviour, C.R. (2004). Review of experimental techniques for high rate deformation and shock studies: International Journal of Impact Engineering, **30**(7): 725-775.

Hart, R., Cundall, P.A., and Lemos, J. (1988). Formulation of a three-dimensional distinct element model—Part II. Mechanical calculations for motion and interaction of a system composed of many polyhedral blocks. International Journal of Rock Mechanics and Mining Sciences & Geomechanics Abstracts, **25**(3):117-125.

He, M.C., Xie, H.P., Peng, S.P., and Jiang, Y.D. (2005). Study on rock mechanics in deep mining engineering. Chinese Journal of Rock Mechanics and Engineering, **24**(16): 2803-2813.

He, M., Miao, J., Li, D., and Wang, C. (2007). Experimental study on rockburst processes of granite specimen at great depth. Chinese Journal of Rock Mechanics and Engineering, **26**(5): 865-876.

He, M.C., Zhao, F., Cai, M., and Du, S. (2015). A novel experimental technique to simulate pillar burst in laboratory. Rock Mechanics and Rock Engineering, **48**(5): 1833-1848.

Hu, Q.T., Zhou, S.N., and Zhou, X.Q. (2008). Mechanical mechanism of coal and gas outburst process. Journal of the China Coal Society, **33**(12): 1368-1372.

Huang, L.X. (2011). Development and new achievements of rock dynamics in China. Rock and Soil Mechanics, **32**(10): 2889-2900.

Huang, Z., Tang, C.A., Ma, T., and Tang, L. (2011). Numerical test investigation on unloading rockburst processes. Chinese Journal of Rock Mechanics and Engineering, **30**(1): 3120-3128.

Johnson, K. L., O'Connor, J. J., and Woodward, A. C. (1973). The effect of the indenter elasticity on the hertzian fracture of brittle materials. Series A, Mathematical and Physical Sciences, **334**: 95-117.

Kimberley, J., Ramesh, K.T., and Barnouin, O.S. (2010). Visualization of the failure of quartz under quasistatic and dynamic compression. Journal of Geophysical Research: Solid Earth, **115**: B08207.

Li, M., Mao, X., Cao, L., Mao, R., and Pu, H. (2015). Experimental study on mechanical properties of coal under high strain rate. Journal of Mining and Safety Engineering, **32**(2): 317-324.

Li, X., Li, D., Guo, L., and Ye, Z. (2007). Study on mechanical response of highly-stressed pillars in deep mining under dynamic disturbance. Chinese Journal of Rock Mechanics and Engineering, **26**(5): 922-928.

Li, X.B., Lok, T.S., and Zhao, J. (2005). Dynamic characteristics of granite subjected to intermediate loading rate. Rock Mechanics and Rock Engineering, **38**(1): 21-39.

Lu, W., Chen, M., Yan, P., and Zhou, C. (2007). Study on vibration characteristics of surrounding rock induced by tunnel excavation under high in-situ stress. Chinese Journal of Rock Mechanics and Engineering, **26**(1): 3329-3334.

Lu, W., Yang, J., Yan, P., Chen, M., Zhou, C., Luo, Y., and Jin, L. (2012). Dynamic response of rock mass induced by the transient release of in-situ stress. International Journal of Rock Mechanics and Mining Sciences, **53**(0): 129-141.

Lu, W., Zhou, C., Chen, M., Jin, L., and Yan, P. (2008). Research on transient characteristics of excavation unloading. Chinese Journal of Rock Mechanics and Engineering, **27**(11): 2184-2192.

Michelle, L.C., and Erland, M.S. (1994). The cracking of ice during rapid unloading. Philosophical Magazine Letters, **69**: 9-14.

Poncelet, E.F. (1946). Fracture and comminution of brittle solids. Transactions American Institute of Mining and Metallurgical Engineering, **169**: 37-57.

Shao, P., Zhang, Y., and He, Y.N. (2004). Rockburst mechanism of random resonance. Journal of the China Coal Society, **29**(6): 668-671.

Tao, M., Li, X., and Li, D. (2013). Rock failure induced by dynamic unloading under 3D stress state. Theoretical and Applied Fracture Mechanics, **65**(0): 47-54.

Tao, M., Li, X., and Wu, C. (2012). Characteristics of the unloading process of rocks under high initial stress. Computers and Geotechnics, **45**(0): 83-92.

Tonge, A.L., Kimberley, J., and Ramesh, K.T. (2012). The mechanism of compressive unloading failure in single crystal quartz and other brittle solids. International Journal of Solids and Structures, **49**(26): 3923-3934.

Wei, J., Zhu, W.C., Niu, L.L., and Wei, C.H. (2014). Finite element analysis of transient unloading and plastic zone distribution in surrounding rock. Journal of Northeastern University, **35**(1) 117-121.

Xu, H., and Lu, W. (2003). Study on dynamic unloading effect during process of fragmentizing rock by blasting. Rock and Soil Mechanics, **24**: 970-974.

Yan, P., Lu, W.-b., Chen, M., Hu, Y.G., Zhou, C.B., and Wu, X.X. (2015). Contributions of in-situ stress transient redistribution to blasting excavation damage zone of deep tunnels. Rock Mechanics and Rock Engineering, **48**(2): 715-726.

Yang, D., Li, H.-B., Xia, X., and Luo, C.W. (2014). Study of blasting-induced dynamic damage of tunnel surrounding rocks under high in-situ stress. Rock and Soil Mechanics, **35**(4): 1110-1116+1122.

Yang, J., Lu, W., Chen, M., Yan, P., and Zhou, C. (2013). Microseism induced by transient release of in-situ stress during deep rock mass excavation by blasting. Rock Mechanics and Rock Engineering, **46**(4): 859-875.

Yi, C.P., Lu, W.-B., Xu, H.T., and Zhou, C.B. (2005). Study on effects of dynamic unloading on initial stress during rock excavation. Chinese Journal of Rock Mechanics and Engineering, **24**: 4750-4754.

Submitted: 04/12/2017
Revised: 27/12/2018
Accepted: 15/03/2018

تحليل التأثير الديناميكي وموجة الإجهاد عن طريق التفريغ العابر لعينة من الصخور تحت ظروف الإجهاد العالية

[1،2]هونغ يون يانغ، [1]شوقانغ تساو، [2]غيسونغ زهو، [1]يونغ لي، [1]رويكاي بان، [1]يوان تشاو
[1]مختبر الدولة الرئيسي لديناميكيات والتحكم في كوارث مناجم الفحم، جامعة تشونغتشينغ، الصين
[2]شركة جيزوبا للمتفجرات، المحدودة، تشونغتشينغ، الصين
المؤلف: *shugang.cao@cqu.edu.cn*

الملخص

تم الحصول على معادلة معدل الإجهاد لعينة صخرية أثناء عملية التفريغ العابرة، وأشار حجم معدل الإجهاد إلى أن عينة الصخور كان لها تأثير ديناميكي واضح وفقاً لمعيار معدل الإجهاد لديناميكيات تحميل الصخور. وفي الوقت نفسه، فإن وحدة النهاية أنتجت إجهاد الشد بأوقات تفريغ محددة. علاوة على ذلك، تم استخدام الوحدة الديناميكية لبرنامج 3DEC وطريقة حساب «البدء بالإجهاد الثابت – التفريغ الديناميكي» لتحليل خاصية انتشار الإجهاد بعد التفريغ العابر. وقد لوحظ أن عينة الصخور التي تحتوي على مادة مرنة قد أنتجت إجهاد شد عالي وإجهاد ضاغط والذين قد انعكسا على طرفي العينة، وكانت فترة الدورة 4 × T عندما كان وقت الإنتشار بين الطرفين هو T. بالإضافة إلى ذلك، أظهرت عينة الصخور ذات المواد البلاستيكية المرنة منطقة تلف البلاستيك التي تأثرت بإجهاد الشد، والذي تم إنتاجه عن طريق الانعكاس عند طرف ثابت. وأخيراً، أظهرت النتائج أن الإجهاد الداخلي كان دائماً إجهاد الشد وأن إجهاد الضغط لم يظهر أبداً بعد إنتاج منطقة التلف. وفي نفس الوقت، كانت فترة دورة إجهاد الشد 2 × T وأن الإجهاد يمثل ظاهرة الإضعاف.